Numerical modeling of propagation of breaking nonlinear acoustic-gravity waves from the lower to the upper atmosphere

Article *in* Advances in Space Research · February 2013

DOI: 10.1016/j.asr.2012.10.023

CITATIONS
11

READS
79

2 authors:

Nikolai M. Gavrilov
Saint Petersburg State University
223 PUBLICATIONS **1,082** CITATIONS
SEE PROFILE

Sergey Kshevetskii
Immanuel Kant Baltic Federal University
71 PUBLICATIONS **180** CITATIONS
SEE PROFILE

Manuscript submitted to "Advances in Space Research"
Final edited version - see Advances in Space Research, v. 51, No. 7, 1168-1174, 2013
http://www.sciencedirect.com/science/article/pii/S0273117712006734

NUMERICAL MODELING OF PROPAGATION OF BREAKING NONLINEAR ACOUSTIC-GRAVITY WAVES FROM THE LOWER TO THE UPPER ATMOSPHERE

Nikolai M. Gavrilov[1], Sergey P. Kshevetskii[2],

[1]Atmospheric Physics Department, Saint-Petersburg State University, Saint-Petersburg, Russia
[1]Theoretical Physics Department, Immanuel Kant Baltic Federal University, Kaliningrad, Russia

Abstract.
Acoustic-gravity waves (AGWs) observed in the upper atmosphere may be generated near the Earth's surface due to a variety of meteorological sources. Two–dimensional simulations of vertical propagation and breaking of nonlinear AGWs in the atmosphere are performed. Forcing near the Earth's surface is used as the AGW source in the model. We use a numerical method based on finite–difference analogues of fundamental conservation laws for solving atmospheric hydrodynamic equations. This approach selects physically correct generalized solutions of the wave hydrodynamic equations. Numerical simulations are performed in a representative region of the Earth's atmosphere up to altitude 500 km. Vertical profiles of temperature, density, molecular viscosity and heat conductivity were taken from the standard atmosphere model MSIS-90 for January. Calculations were made for different amplitudes and frequencies of lower boundary wave forcing. It is shown that after activating the tropospheric wave forcing, the initial pulse of AGWs may very quickly propagate to altitudes of 100 km and above and relatively slowly dissipate due to molecular viscosity and heat conduction. This may increase the role of transient nonstationary waves in effective energy transport and variations of atmospheric parameters and gas admixtures in a broad altitude range.

1. Introduction.

Acoustic-gravity waves (AGWs) frequently observed in the upper atmosphere are generated at tropospheric heights (Fritts and Alexander, 2003). By propagating upward, AGWs can break creating irregularities and turbulence in the upper atmosphere. The majority of tropospheric AGW sources are nonstationary random processes. Some AGW sources may be connected with mesoscale convection and turbulence in the troposphere (Fritts and Alexander, 2003; Fritts et.al., 2006). These sources may be maximized at altitudes of tropospheric jet streams at 9–12km (Medvedev and Gavrilov, 1995; Gavrilov and Fukao, 1999; Gavrilov, 2007).

Baker and Schubert (2000) studied propagation and breaking of nonlinear AGWs in Venus atmosphere. They simulated propagation of waves in a rectangular atmospheric region with horizontal and vertical dimensions of 120 and 48 km, respectively. Other authors (Fritts and Garten, 1996; Andreassen et al., 1998; Fritts et al., 2009, 2011) simulated the effects of atmospheric internal wave breaking and Kelvin-Helmholtz instabilities. Their models were three-dimensional and simulated wave propagation and breaking in rectangular regions with limited horizontal and vertical dimensions. To solve hydrodynamic equations, the authors searched for solutions as Galerkin-type series, using a modification of the spectral method in order to turn

hydrodynamic equations into ordinary differential (versus time) equations for coefficients of the spectral series. Two-dimensional numerical models of atmospheric AGWs were recently developed by Yu and Hickey (2007) and Liu et al. (2008).

Besides numerical studies, propagation and dissipation of small-scale internal gravity waves of lower atmospheric origin have recently been studied in a three-dimensional comprehensive general circulation model [Yiˇgit et al., 2009, 2012] incorporating an extended gravity wave parameterization that accounts for nonlinear saturation as well as dissipation of gravity waves in the thermosphere [Yiˇgit et al., 2008].

In the present paper, we solve atmospheric hydrodynamic equations using a two-dimensional numerical method described by Kshevetskii and Gavrilov (2005) and based on finite-difference analogues of fundamental conservation laws. This approach provides conservatism of the numerical method, allowing consideration of non-smooth solutions of nonlinear dynamic equations. This allows us to select physically correct generalized solutions of the equations (Lax, 1957; Richtmayer and Morton, 1967). But the algorithm is quite complicated and computer time consuming. Therefore, Kshevetskii and Gavrilov (2005) have made only a few examples of calculations of nonlinear gravity wave propagation in the atmosphere. Developments in computers and computational techniques have enabled a substantial reduction in computer time requirements for such problems. In the present study, we make a more extensive simulation of the propagation of nonlinear breaking AGWs from tropospheric sources into the upper atmosphere using the algorithm by Kshevetskii and Gavrilov (2005).

In our non-hydrostatic model, AGWs are forced by specifying monochromatic sinusoidal variations of vertical velocity at the lower boundary. We may expect that if the amplitude of excitation is sufficiently small, the solution should correspond to a linear AGW theory. Thus, near the source the wave may remain harmonic, but its amplitude should increase with height and nonlinearity of hydrodynamic equations may become significant at high altitudes. In the present paper, we study dependences of nonlinear wave effects in the middle and upper atmosphere on the amplitudes and frequencies of wave forcing for a fixed horizontal phase speed.

2. Simulation method.

The two-dimensional numerical model of nonlinear acoustic-gravity waves in the plain atmosphere calculates horizontal u and vertical w components of velocity along horizontal and vertical axes x and z, respectively. It also computes deviations of temperature T', pressure p' and density ρ' from stationary background values T_0, p_0 and ρ_0, respectively. The set of two-dimensional nonlinear hydrodynamic equations of our model is described by Kshevetskii and Gavrilov (2005) and includes primitive equations of continuity, motion and heat balance. We set the upper boundary conditions as zero vertical gradients of temperature and horizontal velocity, also zero vertical velocity at altitude z = 500 km. The lower boundary conditions are zero horizontal velocity and temperature deviations at the Earth's surface (see Kshevetskii and Gavrilov, 2005). The lower boundary condition for w is the source of waves in the model. In the present study we assume a form of monochromatic plane wave

$$(w)_{z=0} = W_0 \cos[\sigma\,(t - x/c)], \qquad (1)$$

where σ and c are frequency and horizontal wave speed, respectively; W_0 is the wave forcing amplitude. Eq. (1) may represent, for example, spectral components of convective, orographic and turbulent processes, which are considered as important AGW sources in the atmosphere (Fritts et al., 2006). In the horizontal direction we assume periodicity of wave solutions in the following form

$$f(x, z, t) = f(x+L, z, t), \quad (2)$$

where f denotes any of the calculated hydrodynamic variables, and L is the horizontal dimension of the atmospheric domain for our numerical modeling. The numerical scheme used in our model is described by Kshevetskii and Gavrilov (2005). It is a modification of the well-known two-step Lax–Wendroff (1960) scheme. This scheme takes into account the hydrodynamic conservation laws of density, momentum and energy. The main mathematical difference between our scheme and the classical Lax and Wendroff (1960) one is the usage of an implicit approximation at first time half step. In this case, it has been shown that the errors from acoustic waves are not accumulated with time for finite-difference schemes of such a structure (Kshevetskii, 2001a, b, c). One more peculiarity of our scheme is usage of a staggered (‘‘chess’’) grid, in which different hydrodynamic variables are calculated at spatial locations on different subgrids.

Present simulations are carried out for background vertical profiles of T_0, p_0 and ρ_0 taken from the standard atmosphere model MSIS-90 [Hedin, 1991] for January at moderate geomagnetic activity. AGW calculations are made for different parameters in Eq. (1) for the lower boundary forcing. The average vertical grid step in our calculations is about 250 m, but it automatically varies with altitude depending on the inhomogeneity of the background wind and temperature profiles. Horizontal grid and time steps depend on the parameters of the wave forcing. In the present paper we make calculations for different frequencies σ and only one value of phase speed c = 100 m/s at lower boundary. A rather big value of c has been chosen as a representative of fast AGWs. Convective activity in the troposphere and strong tsunamis can produce waves with comparably large phase speeds [Hickey et al., 2009]. General circulation modeling studies of Yiğit et al. [2009, 2012] and Yiğit and Medvedev [2009, 2010] based on the extended gravity wave parameterization by Yiğit et al. [2008] with an initial GW spectrum including harmonics up to c = ±80 m/s showed that gravity waves of lower atmospheric origin penetrate into the thermosphere up to F region altitudes, generating appreciable dynamical and thermal effects on the upper atmosphere.

Inconsistent initial conditions can give birth to severe acoustic waves, which may be transformed into shock waves because of equation nonlinearity. This may cause significant computational difficulties. In order to filter out the initial acoustic waves, we solve the linearized equations first, and then use the obtained propagating wave as the initial condition to the nonlinear problem. In this way, the acoustic waves may be further generated only due to nonlinear effects, their amplitudes are relatively small, and generation of shock waves is practically impossible.

Molecular viscosity and heat conductivity are not practically important for long wave disturbances propagating in the atmosphere below altitude 100 km, but they may become important higher. Therefore, our numerical model takes molecular viscosity and heat conductivity into account. The model omits some physical effects that seem to be of secondary importance for studying nonlinear atmospheric waves.

3. **Results of calculations.**

Calculations using the described numerical model were made from zero initial conditions starting from the moment $t = 0$ of activating the lower boundary wave forcing. In Eq. (1) we used different frequencies σ and fixed $c = 100$ m/s. For each σ we take the horizontal dimension of the atmospheric domain for modeling $L = 4\lambda_x$, where $\lambda_x = 2\pi c/\sigma$ is the horizontal wave length.

Medvedev and Gavrilov (1995) studied mechanisms of AGW generation due to nonlinear interactions in meteorological and turbulent motions in the troposphere. They showed that such interactions may produce wave spectral components with broad ranges of amplitudes and other parameters. Figure 1 shows calculated fields of wave perturbations of temperature T' at different times after activating the lower boundary wave forcing Eq. (1) with $\sigma = 10^{-4}$ s^{-1}, c = 100 m/s and

a low amplitude W_0 = 0.1 cm/s. One can see that just after activating the wave forcing at the Earth's surface, acoustic waves are generated and propagate upwards. In the horizontally periodical case under consideration, these acoustic perturbations have the form of vertically propagating disturbances as shown in Figures 1a-c for different time moments *t* just after activating the wave forcing. These disturbances propagate with the speed of sound and in a few minutes may reach altitudes of 100 km and above. Their amplitudes increase at high altitudes, where acoustic waves may produce substantial perturbations. These initial acoustic waves dissipate due to molecular viscosity and heat conduction. This process is not fast and may require a few wave periods. After that, the surfaces of constant phases at low altitudes become inclined to the horizontal at angles $\alpha \sim \arcsin(\sigma/N)$, where N is the Brunt-Vaisala frequency, in accordance with AGW theory (Gossard and Hooke, 1975). Such inclined AGW structures one can see in Figure 1d after 20 hours of in-model time. Above altitude 100 km molecular viscosity and heat conduction increase and angles α increase in the upper part of Figure 1d.

Figure 2 shows the distributions of horizontal and vertical velocity, and temperature deviations at t = 20 hr for the same wave mode as Figure 1, but with a 10-fold increase in the amplitude of lower boundary forcing. One can see small-scale structures above altitude 80 km, which are produced due to wave instability. Kshevetskii and Gavrilov (2005) analyzed the kinds of instabilities in the two-dimensional numerical model of nonlinear IGWs. They showed that at moderate forcing amplitude, the wave can break mainly due to Kelvin-Helmholtz instability of the wind shears created by the propagating wave. Convective instability could be a reason for wave breaking at large forcing amplitudes.

When the amplitude of the wave forcing increases 10 times more, wave instability and small-scale structures appear at lower altitudes (see Figure 3). But wave amplitudes of temperature perturbations at altitudes 160 – 200 km in Figures 1c and 3c have almost the same magnitudes despite a 100 times difference in the lower boundary wave forcing. Comparison of Figure 2 and 3 reveals 2 and 4-times increases in amplitudes of horizontal and vertical velocity perturbations, respectively, at altitudes 160 – 200 km. These values are much smaller than the 10 times increase in W_0 (see Eq. (1)) between Figures 2 an 3.

This behavior is consistent with the hypothesis of wave saturation (Fritts and Alexander, 2003), according to which nonlinear effects and instabilities may lead to increased dissipation of AGW energy propagating from below and may stabilize wave amplitudes in the upper atmosphere. Usually AGW saturation is considered in relation to wave breaking into small-scale turbulence (Lindzen, 1981). Horizontal and vertical grid steps of our numerical model (see section 2) are not sufficient to resolve small-scale turbulence. Therefore, irregularities in Figures 2 and 3 are connected with medium scale convection and dynamical instabilities caused by the initial nonlinear wave. Larger gradients of velocity and temperature lead to an increase in wave energy dissipation due to molecular viscosity and heat conduction in our model and to a slowdown of the initial wave rise with height. So conditions for wave saturation in the atmosphere may be produced not only by small-scale turbulence, but also by mesoscale irregularities produced by nonlinear unstable AGWs.

Figure 4 is calculated for the same model parameters as Figure 3 but with the wave forcing having frequency $\sigma = 10^{-3}$ s^{-1}. One can see that the main maxima and minima of all hydrodynamic variables in Figure 4 are located lower and have smaller magnitudes than that in Figure 2. According to standard AGW theory, the vertical component of horizontal wave momentum flux at lower boundary produced by the forcing described by Eq. (1) has the form of

$$F_{mz} = \rho_0 N W_0^2/(2\sigma). \qquad (3)$$

Wave momentum flux is proportional to total wave energy flux and to wave action flux (see Gavrilov and Fukao (1999)). According to Eq. (3), 10 times larger σ for wave shown in Figure 4 compared to that in Figure 3 at the same other conditions leads to 10 times smaller wave

momentum flux entering the atmosphere from the lower boundary. This may explain the decrease in AGW amplitudes in Figure 4 compared to Figure 3.

Figures 5 and 6 show the same fields as Figure 2, but for higher frequency lower boundary wave forcing $\sigma = 10^{-2}$ s^{-1} and amplitudes $W_0 = 0.1$ cm/s and $W_0 = 1$ cm/s, respectively. Comparison of these Figures reveals that at altitudes 100-160 km the amplitudes of temperature perturbations in Figure 6c are even smaller than those in Figure 5c despite a 10 times larger amplitude of the lower boundary forcing. The same effect can be seen in Figures 6b and 5b for vertical velocity. Similarly to Figures 1 – 3 this shows that higher amplitudes of lower boundary forcing may lead to more intensive nonlinear destruction and dissipation of wave energy, so that wave amplitudes in the upper atmosphere could become even smaller at higher forcing amplitudes. Figures 5a and 6a show an increase in horizontal velocity averaged over the wave period. This effect is more noticeable in Figure 6a for higher amplitudes of the lower boundary wave forcing Eq. (1).

Changes in the mean horizontal velocity caused by dissipating waves are well known effects (see, for example, Fritts and Alexander, 2003). They were demonstrated with other nonlinear AGW models (for example, Liu et al., 2008). Dissipating nonlinear AGWs may produce accelerations of the mean flow, which are considered as an important factor in the formation of general circulation of the middle and upper atmosphere (see Lindzen, 1981). Energy transfer from AGW to the mean wind may form wave-induced jets at altitudes of increased dissipation of the propagating wave as it is seen in Figures 5a and 6a. Comparison of Figures 1a – 6a for different frequencies and amplitudes of the lower boundary excitation Eq.(1) shows that at the same amplitude of the wave forcing, higher frequency waves may produce larger dynamical effect on the mean wind in the middle and upper atmosphere.

Figure 1 shows substantial initial acoustic waves, which propagate very quickly into the upper atmosphere and dissipate there due to molecular viscosity and heat conduction (see above). Our modeling showed that this dissipation process is not quick and usually requires several wave periods (see Figure 1). During this interval we may have a transition from the initial acoustic pulse to a developed structure of stationary acoustic gravity waves being generated by the lower boundary excitation Eq. (1). During this transitional period, parameters of the wave fields are not stationary. Experiments (Fritts and Alexander, 2003) frequently observe relatively short pulses continuing for a few AGW wavelengths and periods in the atmosphere. This means that many AGW sources in the atmosphere may work for a relatively short time (Fritts et al., 2006). If such irregular wave sources quickly appear and disappear due to convective and dynamical instabilities and other processes in the atmosphere, they may produce acoustic and gravity wave pulses, which will not have enough time to become stationary during the time of the wave source's activity.

This allows us to assume that a substantial part of AGWs observed in the atmosphere may be non-stationary. This may raise a question to what extent the usual theory of stationary AGWs, frequently used for description of AGWs in the atmosphere, may be applicable to nonstationary AGWs. We have presented three calculations by increasing the amplitude of AGW forcing at the lower boundary by a factor of 10 in each simulation, which sometimes may exceed the strength of tropospheric wave sources observed in the atmosphere. The representative amplitudes that have been tested in the present study help to better understand the response of atmospheric wave propagation and the resulting perturbations to possible variations in lower atmospheric wave sources.

Conclusion

Nonlinear AGWs propagating to the middle and upper atmosphere from a harmonic wave forcing of various frequencies and amplitudes near the ground have been simulated numerically. After the tropospheric forcing of atmospheric waves is activated, these waves very quickly propagate to very high altitudes above 100 km and relatively slowly dissipate due to molecular

viscosity and heat conduction. Nonlinear interactions may lead to creation of smaller scale structures and instabilities. These smaller scale structures increase gradients of wave fields and increase the rate of wave dissipation. Therefore, AGW amplitudes in the upper atmosphere may grow much slower than the increase in tropospheric forcing amplitude. Wave dissipation and instabilities lead to wave-induced acceleration of the mean flow and to creation of wave-induced mean flows in the middle and upper atmosphere. Shorter period AGWs seem to be more effective in producing the wave induced mean flows at fixed amplitudes and horizontal wave speeds of the tropospheric wave forcing. Further studies of nonstationary AGWs in the middle and upper atmosphere are required. Numerical models of nonlinear atmospheric AGWs based on primitive hydrodynamical equations may help in studies of AGWs from nonstationary sources in the atmosphere.

Acknowlegements. This work was partly supported by Russian Basic Research Foundation. The authors thank A. N. Gavrilov for help in improving computer code.

References.

Andreassen, O., Hvidsten, O., Fritts, D., Arendt, S. Vorticity dynamics in a breaking internal gravity wave. Part 1. Initial instability evolution. J. Fluid Mech. 367. 27–46. 1998.

Fritts, D.C., Garten, J.F. Wave braking and transition to turbulence in stratified shear flows. J. Atmos. Sci. 53 (8), 1057–1085. 1996.

Fritts, D. C., Alexander, M. J. Gravity wave dynamics and effects in the middle atmosphere. Rev. Geophys. 41. 1. doi:10.1029/2001RG000106. 2003.

Fritts, D. C., Vadas, S. L., Wan, K., Werne, J. A. Mean and variable forcing of the middle atmosphere by gravity waves, J. Atmos. Solar-Terr. Phys. 68. 247–265. 2006.

Fritts, D. C., Wang, L., Werne, J., Lund, T., Wan, K. Gravity wave instability dynamics at high Reynolds numbers. Part II: turbulence evolution, structure, and anisotropy, J. Atmos. Sci., 66, 1149–1171, 2009

Fritts, D. C., Franke, P. M., Wan, K., Lund, T., Werne, J. Computation of clear-air radar backscatter from numerical simulations of turbulence: 2. Backscatter moments throughout the lifecycle of a Kelvin-Helmholtz instability. J. Geophys. Res. 116. D11105. doi:10.1029/2010JD014618. 2011.

Gavrilov, N. M. Structure of the mesoscale variability of the troposphere and stratosphere found from radio refraction measurements via CHAMP satellite. _Izvestia Atmos. Oceanic. Phys. 43(4). 451-460, 2007

Gavrilov, N. M., Fukao, S. A. A comparison of seasonal variations of gravity wave intensity observed by the MU radar with a theoretical model. J. Atmos. Sci. 56. 3485–3494. 1999.

Gossard, E. E., Hooke, W. H. Waves in the atmosphere, Elsevier Sci. Publ. Co., Amsterdam-Oxford-New York, 1975.

Hedin A.E. Neutral atmosphere empirical model from the surface to lower exosphere MSISE-90, Extension of the MSIS thermosphere model into the middle and lower atmosphere, J. Geophys. Res., 96, 1159—1172, 1991.

Hickey, M. P., Schubert, G., Walterscheid, R. L. Propagation of tsunami-driven gravity waves into the thermosphere and ionosphere, J. Geophys. Res., 114. A08304. doi:10.1029/2009JA014105. 2009.

Yi˘git, E., Medvedev, A. S., Heating and cooling of the thermosphere by internal gravity waves, Geophys. Res. Lett., 36, L14807, doi:10.1029/2009GL038507. 2009.

Yi˘git, E., Medvedev, A. S., Internal gravity waves in the thermosphere during low and high solar activity: Simulation study., J. Geophys. Res., 115, A00G02, doi:10.1029/2009JA015106. 2010.

Yi˘git, E., Aylward, A. D., Medvedev, A. S. Parameterization of the effects of vertically propagating gravity waves for thermosphere general circulation

models: Sensitivity study, J. Geophys. Res., 113, D19106, doi:10.1029/2008JD010135, 2008.

Yiˇgit, E., Medvedev, A. S., Aylward, A. D., Hartogh, P., and Harris, M. J. Modeling the effects of gravity wave momentum deposition on the general circulation above the turbopause, J. Geophys. Res., 114, D07101, doi:10.1029/2008JD011132. 2009.

Yiˇgit, E., Medvedev, A. S., Aylward, A. D., Ridley, A. J., Harris, M. J., Moldwin, M. B., Hartogh, P. Dynamical effects of internal gravity waves in the equinoctial thermosphere, J. Atmos. Sol.-Terr. Phys., doi:10.1016/j.jastp.2011.11.014. 2012.

Kshevetskii, S.P. Modelling of propagation of internal gravity waves in gases. Comput. Math. and Math. Phys. 41 (2), 295–310, 2001a.

Kshevetskii, S.P. Analytical and numerical investigation of nonlinear internal gravity waves. Nonlin. Proc. Geophys. 8. 37–53. 2001b.

Kshevetskii, S.P. Numerical simulation of nonlinear internal gravity waves. Comput. Math. and Math. Phys. 41 (12). 1777–1791. 2001c.

Kshevetskii, S. P., Gavrilov, N. M. Vertical propagation, breaking and effects of nonlinear gravity waves in the atmosphere. J. Atmos. Solar-Terr. Phys. 67. 1014–1030. 2005.

Lax, P.D. Hyperbolic systems of conservation laws. Comm. Pure Appl. Math. 10, 537–566. 1957.

Lax, P.D., Wendroff, B. Hyperbolic systems of conservation laws. Comm. Pure and Appl. Math. 13, 217–237. 1960.

Lindzen, R.S. Turbulence and stress owing to gravity wave and tidal breakdown, J. Geophys. Res., 86, 9707-9714, 1981.

Liu, X., Xu, J., Liu, H.-L., Ma, R. Nonlinear interactions between gravity waves with different wavelengths and diurnal tide. J. Geophys. Res.. 113. D08112. doi:10.1029/2007JD009136. 2008.

Medvedev, A. S., Gavrilov, N. M. The nonlinear mechanism of gravity wave generation by meteorological motions in the atmosphere, J. Atmos. Terr. Phys., 57, 1221–1231, 1995.

Richtmayer, R.R., Morton, K.W. Difference Methods for Initial-Value Problems. Intersci. Publ., New York. 1967.

Yu, Y., Hickey, M. P. Numerical modeling of a gravity wave packet ducted by the thermal structure of the atmosphere. J. Geophys. Res. 112. A06308. doi:10.1029/2006JA012092. 2007.

Figure captions.

Figure 1. Calculated temperature deviations (in K) produced by low boundary plane wave forcing with frequency $\sigma = 10^{-4}\,s^{-1}$, horizontal phase speed c = 100 m/s and amplitude W_0 = 0.1 cm/s at times t = 0.05 hr (a), t = 0.1 hr (b), t = 0.5 hr (c), and t = 20 hr (d) after activating the forcing.

Figure 2. Calculated horizontal velocity in m/s (a), vertical velocity in m/s (b) and temperature deviations in K (c) produced by plane wave surface forcing with $\sigma = 10^{-4}\,s^{-1}$, c = 100 m/s and amplitude W_0 = 1 cm/s at time t = 20 hr after switching on the forcing.

Figure 3. Same as Figure 2, but for the amplitude of low boundary wave forcing W_0 = 10 cm/s.

Figure 4. Same as Figure 2, but for the low boundary wave forcing with $\sigma = 10^{-3}\,s^{-1}$, c = 100 m/s and amplitude W_0 = 10 cm/s.

Figure 5. Same as Figure 2, but for the lower boundary wave forcing with $\sigma = 10^{-2}\,s^{-1}$, c = 100 m/s and amplitude W_0 = 0.1 cm/s.

Figure 6. Same as Figure 2, but for the low boundary wave forcing with $\sigma = 10^{-2}\,s^{-1}$, c = 100 m/s and amplitude W_0 = 1 cm/s.

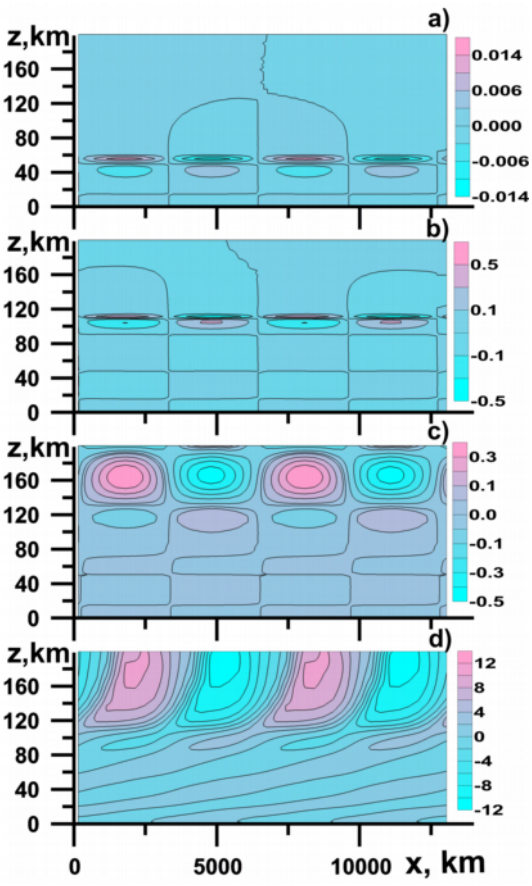

Figure 1. Calculated temperature deviations (in K) produced by low boundary plane wave forcing with frequency $\sigma = 10^{-4}\,s^{-1}$, horizontal phase speed c = 100 m/s and amplitude W_0 = 0.1 cm/s at times t = 0.05 hr (a), t = 0.1 hr (b), t = 0.5 hr (c), and t = 20 hr (d) after activating the forcing.

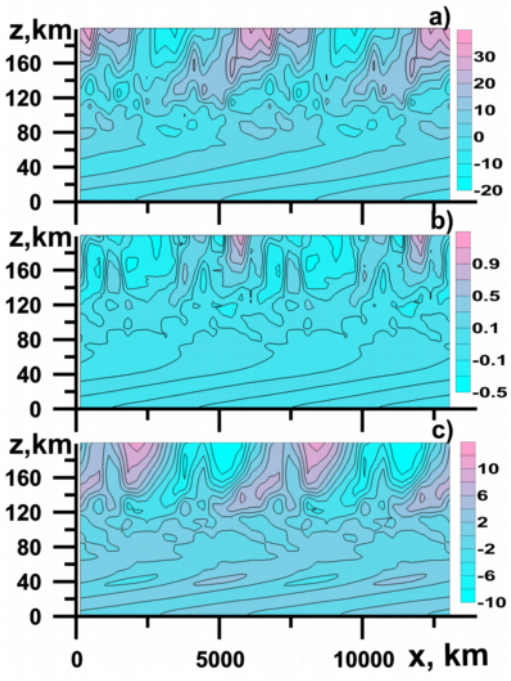

Figure 2. Calculated horizontal velocity in m/s (a), vertical velocity in m/s (b) and temperature deviations in K (c) produced by plane wave surface forcing with $\sigma = 10^{-4}\,s^{-1}$, c = 100 m/s and amplitude W_0 = 1 cm/s at time t = 20 hr after switching on the forcing.

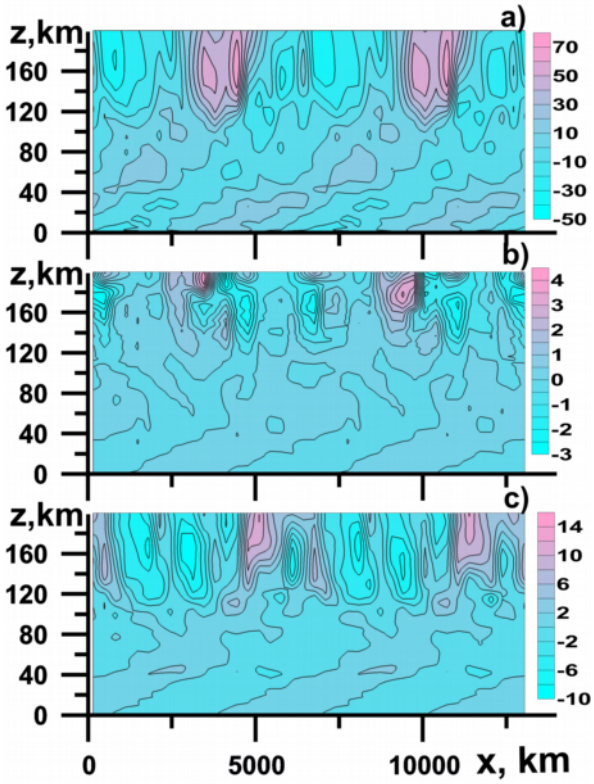

Figure 3. Same as Figure 2, but for the amplitude of low boundary wave forcing W_0 = 10 cm/s.

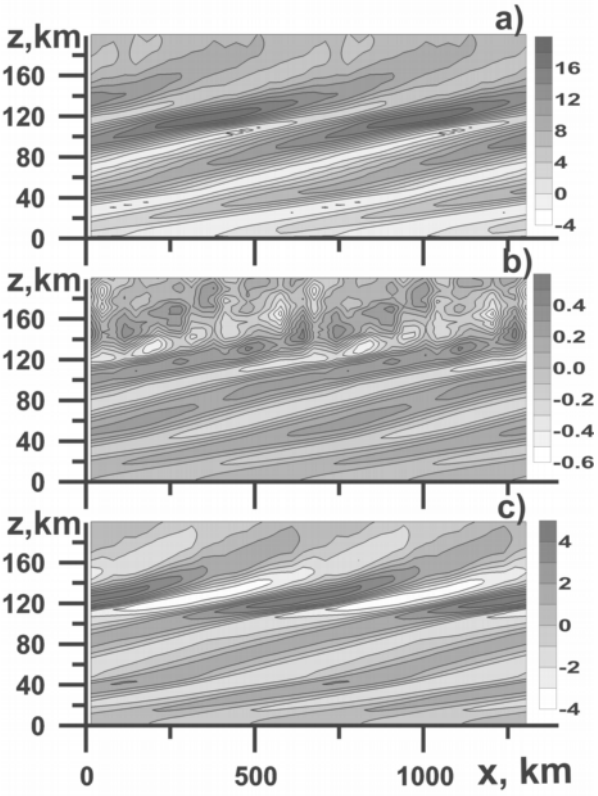

Figure 4. Same as Figure 2, but for the low boundary wave forcing with $\sigma = 10^{-3}\,s^{-1}$, c = 100 m/s and amplitude W_0 = 10 cm/s.

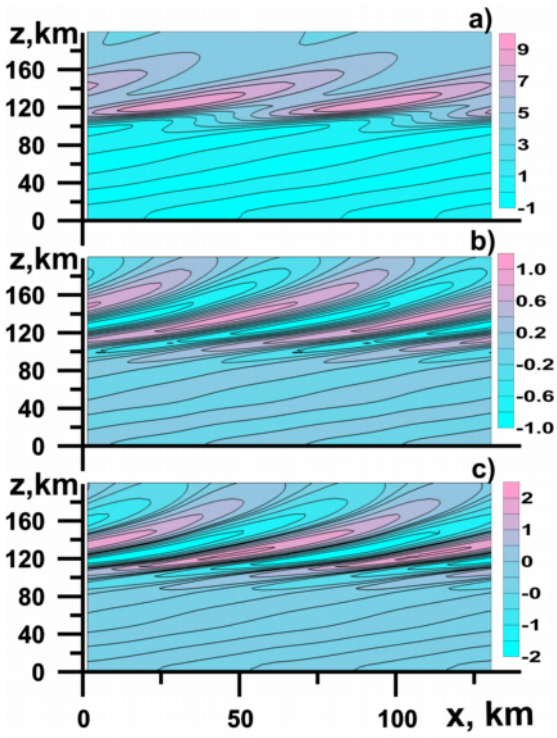

Figure 5. Same as Figure 2, but for the lower boundary wave forcing with $\sigma = 10^{-2}\ s^{-1}$, c = 100 m/s and amplitude W_0 = 0.1 cm/s.

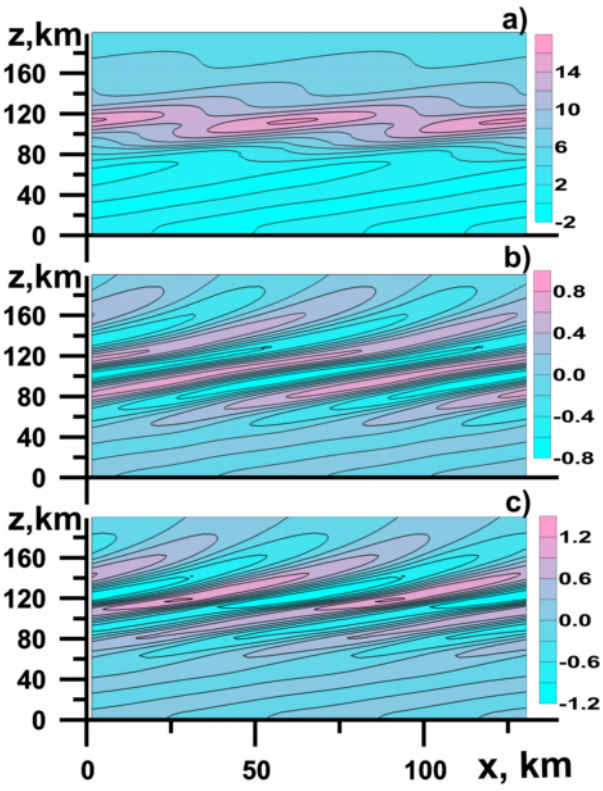

Figure 6. Same as Figure 2, but for the low boundary wave forcing with $\sigma = 10^{-2}\ s^{-1}$, c = 100 m/s and amplitude W_0 = 1 cm/s.